CHEMISTRY OF MATERIALS

Article

pubs.acs.org/cm

On the Location of Host Ca Atoms Responsible for Ferrimagnetism in the Layered Cobaltites $YBaCo_2O_{5.5}$

G. Aurelio,*[,†] F. Bardelli,[‡] R. Junqueira Prado,[¶] R. D. Sánchez,[†,§] M. E. Saleta,[†,§] and G. Garbarino[∥]

[†]CONICET, Centro Atómico Bariloche, 8400 San Carlos de Bariloche, Río Negro, Argentina

[‡]Institut des Sciences de la Terre, Maison des Gèosciences, Grenoble, France

[¶]Instituto de Física, Universidade Federal de Mato Grosso, Cuiabá - MT, Brazil

[§]Instituto Balseiro, Universidad Nacional de Cuyo, Río Negro, Argentina

[∥]European Synchrotron Radiation Facility (ESRF), Grenoble, France

ABSTRACT: Recent studies have shown that the addition of Ca as host ion in the layered compounds $RBaCo_2O_{5+\delta}$ (with R a rare earth or yttrium) produces a dramatic effect on their magnetic properties, as well as on their Seebeck coefficient and resistivity. Studies performed so far have opened up the possibility that the substitution site for Ca atoms might not be obvious, having been reported at the Y site, at the Ba site, or regarded as not decisive to the ferromagnetism enhancement. In this work, we present a comparative study of Ca-doped cobaltite samples synthesized with two different nominal substitution sites, namely, Ca replacing Ba, and Ca replacing Y. X-ray absorption spectroscopy performed at the Ca, Ba, and Co edges to study the local environment around these elements allowed to unequivocally determine that the substitutional site of Ca is the Y site. This important result helps to clarify the mixed valence state of cobalt as Co^{3+} and Co^{4+}, which would be responsible for the ferromagnetic interactions, and explains the antiferromagnetic to ferrimagnetic switch occurring already at 10% Ca doping level.

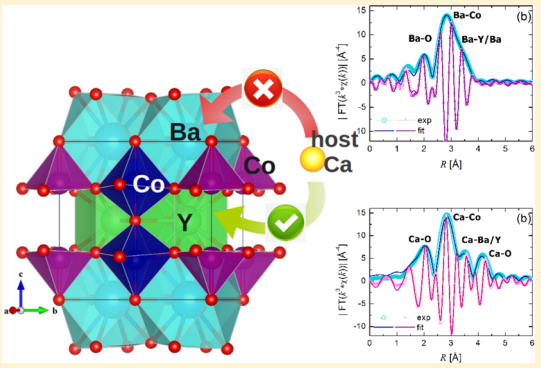

KEYWORDS: *layered cobaltites, X-ray absorption spectroscopy, host cations*

INTRODUCTION

Cobalt-based oxides have been largely studied for their unique properties, not only in basic research for the understanding of their complex magnetic states but also as suitable candidates for numerous applications, from solid oxide fuel cells and batteries to thermoelectric devices, supercapacitors, gas sensors, etc. The layered perovskite compounds $RBaCo_2O_{5+\delta}$ (R being a rare earth) are intensively studied materials, as the mixed valence state of Co ions in these compounds can be controlled by their wide range of oxygen nonstoichiometry. This unique characteristic has provided the scenario for exploring a striking number of promising applications: among the reported properties, we find charge ordering,[1,2] metal−insulator transition,[3−6] magnetic phase separation,[7−11] large thermoelectric power,[12,13] rapid oxygen ion difussion,[14] and a remarkable oxygen storage capability.[15,16]

Lately, a further variable that has been explored in these compounds is the substitution with other cations.[11,17−24] In previous works, we reported that in the Ba-site substituted cobaltites $Y(Ba_{1-x}Sr_x)Co_2O_{5.5}$[10] and $Y(Ba_{1-x}Ca_x)Co_2O_{5.5}$,[6,7] even a small addition of Sr and Ca in the Ba-site (5 to 10%) produces a dramatic effect on the magnetization of the samples, on the Seebeck coefficient, and on the resistivity. In particular, for Ca-substituted samples we found that, although the "122" perovskite crystal structure seems unaffected, the magnetic arrangements of Co ions are drastically modified: the antiferromagnetic (AFM) long-range order is destroyed, and a ferrimagnetic phase with a so-called spin-state order is stabilized below 290 K. Moreover, for $x_{Ca} = 0.05$, a fraction of AFM phase coexists with the ferrimagnetic one below 190 K, whereas for $x_{Ca} = 0.10$ the AFM order is completely lost. Our neutron diffraction studies led us to propose for the parent compound ($x = 0$) a two-phase scenario, which was later confirmed by other authors.[8,9]

Other recent reports on substituted cobaltites[11,12,21,23,24] have opened up the possibility that the substitution site for Ca atoms might not be obvious. Motin Seikh et al.[23] presented a study of the $(Y_{0.9}Ca_{0.1})BaCo_2O_{5.5}$ compound showing very similar magnetic properties as our $Y(Ba_{0.9}Ca_{0.1})Co_2O_{5.5}$ samples. More recently, Sarkar et al.[11] took one step further and compared both cases, studying samples with the two possible nominal substitution sites. The authors obtained a single phased layered perovskite in both cases, with no segregated phases, and concluded that both substitution sites seem to be possible and lead to the same effect in the magnetic state of the samples, which they defined as a magnetic glass.

Received: April 27, 2013
Revised: July 19, 2013
Published: August 6, 2013

Layered cobaltites are known to allow the accommodation of cations with a wide range of ionic radii at the lanthanide *R* site, which, in addition to the wide oxygen nonstoichiometry range and the three possible valence states for Co, renders an extreme versatility to the formation of the compound. However, when substitutions cause a shift in the nominal valence of cobalt, the magnetic interactions can be severely affected. For this reason, although it may be possible for Ca to occupy two different crystallographic sites in the structure, the resulting charge balance may completely modify the magnetic properties.

In order to shed light on the actual substitution site for Ca atoms in the perovskite structure, we undertook an investigation using element−selective tools. The aim of the present work is to better understand the effects of the Ca substitution on the magnetism of the system and on the stability of different structural configurations. To do this, we fine-tuned the synthesis of the oxide to guarantee cation homogeneity, performed synchrotron XRPD (X-ray powder diffraction) to check the long-range crystal structure, and XAS (X-ray absorption spectroscopy) as a chemically selective tool for studying the atomic arrangements at a local scale.

EXPERIMENTAL METHODS

Synthesis. Polycrystalline samples of nominal $(Y_{0.9}Ca_{0.1})BaCo_2O_{5.5}$ (hereafter called YCa10) and $Y(Ba_{0.9}Ca_{0.1})Co_2O_{5.5}$ (alias BaCa10) were prepared by the Pechini sol−gel method,[25] in order to improve homogeneity and cation distribution with respect to the solid−state synthesis method. Citric acid was dissolved in distilled water and stoichiometric amounts of $Co(NO_3)_2{\cdot}6H_2O$ and previously dried Y_2O_3, $BaCO_3$, and $CaCO_3$ were added to the solution in a molar ratio 7:1 of citric acid/cobalt. The solution was stirred and heated on a hot plate at 80 °C for a few hours; then, ethylene glycol was added in a 1:1 citric acid/ethylene glycol molar ratio. The solution was held in the hot plate at 110−120 °C under constant stirring to induce esterification. A clear pink gel was thus obtained, which was dried at 100 °C for 50 h, then ground and calcined at 450 °C in air for 3 h to obtain an amorphous precursor. The precursors were pressed into pellets and sintered at 1000 °C under oxygen flow for 25 h, then repeated to obtain the final products, as shown in Figure 1. The

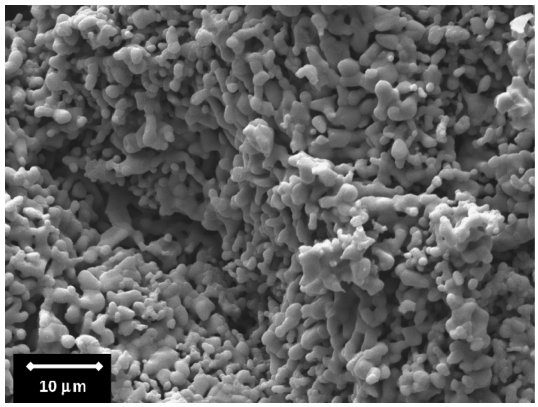

Figure 1. Scanning electron micrography for sample BaCa10 $(Y(Ba_{0.9}Ca_{0.1})Co_2O_{5.5})$.

samples were slowly cooled (1°/min) in the furnace always under oxygen flow, which results in an oxygen content of $\delta = 0.5$, as previously reported.[6,7] The nominal composition of the samples was confirmed by energy dispersive X-ray spectroscopy using a scanning electron microscope Philips 515 equipped with an EDAX analyzer. Magnetic and electrical transport measurements (not shown in this paper) were performed to check the behavior of the new samples in comparison with those previously reported,[6,7] yielding the same results.

X-ray Diffraction. XRPD measurements were performed at room temperature and ambient pressure on the ID27 beamline at the ESRF (Grenoble, France) using a monochromatic microfocused beam with a wavelength $\lambda = 0.3738$ Å. A MARCCD 165 2D detector was used, located at 190 mm from the sample. The collecting time of each pattern was of 10−20 s. Experimental raw data were reduced using the FIT2D program[26] to obtain one-dimensional diffractograms. Analysis of the diffraction data was performed using the Rietveld method implemented in the Fullprof suite software package.[27]

X-ray Absorption Spectroscopy. X-ray absorption near edge structure (XANES) and extended X-ray absorption fine structure (EXAFS) spectra at the calcium K-edge (4038.5 eV) were collected in fluorescence mode using the XAFS2 beamline at LNLS (Campinas-SP, Brazil). EXAFS spectra were acquired with a resolution of 0.3 eV in the near edge (XANES) region (4030 to 4150 eV), while the EXAFS region extended up to 4400 eV. The acquisition was done using an 8-elements Ge fluorescence detector and integrating each energy point for up to 40 s. A double-crystal monochromator, equipped with two silicon (1 1 1) single crystals, was used. Energy was calibrated using a Ti foil, together with CaO and $CaCO_3$ reference samples, as CaO exhibits a pre-edge peak at 4043 eV and $CaCO_3$ exhibits a subpeak at 4059 eV.[28] All scans were collected at room temperature and ambient pressure.

The L_I and L_{III}-Ba absorption edges (5989 and 5247 eV, respectively) were also measured at the XAFS2 beamline at LNLS in transmission mode using 10 mg of sample dissolved in ethanol and deposited on porous polycarbonate membranes.

XANES spectra at the L_I Ba-edge were acquired in the energy interval 5220−5350 eV, with a maximum resolution of 0.5 eV in the near edge region (5240 to 5270 eV). EXAFS spectra at the L_{III} Ba-edge were acquired in the energy interval 5950−6600 eV, with a maximum resolution of 0.5 eV in the near edge region (5990 to 6020 eV), while the EXAFS region extended up to 6600 eV.

Measurements at the Co K-edge were performed in the BM08 beamline (GILDA[29]) at the European Synchrotron Radiation Facility (ESRF) (Grenoble, France). Data were collected in transmission geometry using ionization chambers filled with nitrogen and/or argon gas at pressures suitable to absorb 20% of the upstream beam and 80% of the downstream one at the working energy. A Co foil was measured simultaneously with the samples' spectra for precise energy calibration. The energy sampling interval in the XANES region (7710−7760 eV) was 0.2 eV. Seven-second integration-time energy scans per sample were acquired, interpolated, and averaged in order to increase the signal-to-noise ratio. The estimated energy resolution was of about 0.5 eV. In order to reduce the damping of the signal due to the thermal contribution, the samples were measured at the liquid nitrogen temperature (77 K). A reference compound for Co^{3+} ($LaCoO_3$) was also measured. The samples and reference compounds were prepared to obtain an edge step as close as possible to 1 and to keep the total absorption in the range 1−2.5. Samples were dissolved in ethanol, deposited on porous polycarbonate membranes, and sealed with Kapton tape after drying. Samples were then mounted on a copper sample holder, placed in a vacuum chamber (10^{-5} mbar), and cooled to 77 K.

Standard procedures were followed to extract the EXAFS signal,[30] that is, subtraction of the pre-edge background, normalization, alignment and energy calibration, and spline modeling of the postedge atomic background. EXAFS signals at the Ca and Ba edges were Fourier filtered to exclude contributions of noise and coordination shells above the fourth.

The extraction of the EXAFS signal and the structural refinements were performed using a dedicated software package written in FORTRAN,[31−33] which is based on the MINUIT minimization routines developed at CERN.[34] Minimizations were conducted in the back-Fourier transformed wave vector space. The number of free parameters in the fits never exceeded the number of independent points ($N_{ind} = (2\Delta k \Delta R)/\pi + 1$). The amplitude and phase photoelectron functions were calculated *ab initio* using the FEFF8

dx.doi.org/10.1021/cm401394x | *Chem. Mater.* 2013, 25, 3307−3314

code.[35] The crystallographic clusters centered on the absorption species (Ca, Ba, or Co) used for FEFF calculations were obtained from the structure refined from X-ray diffraction data, which is described in the Results section.

XANES Simulations. XANES spectra at the Ca K-edge were simulated using the *ab initio* FEFF8.4 code.[30,35−37] The full multiple scattering (FMS) and self-consistent-field (SCF) atomic potential calculation routines were found to be crucial to obtain good simulations. After some tests, the Hedin−Lundqvist exchange potential was chosen[38] and used in all calculations with an imaginary part of 0.5 eV to simulate experimental broadening. For the calculation of the SCF muffin-tin atomic potential a cluster of size 6.8 Å (110 atoms) was used. A cluster of 296 atoms was used for the calculation of the FMS.

RESULTS AND DISCUSSION

X-ray Powder Diffraction. As a first step to investigate the location of host Ca atoms in the structure of the layered cobaltites, we performed simulations of X-rays diffractograms to analyze the effect of the substitution under different conditions. Simulations were performed using the *Pmmm* space group, as previously reported.[7] In the first model (labeled Ca@Y in the following), the occupation of the 2*p* Wyckoff site was set to 90% Y + 10% Ca and that of the 2*o* Wyckoff site was set to 100% Ba. In the second model (Ca@Ba in the following), the occupation of the 2*o* Wyckoff site was set to 90% Ba + 10% Ca and that of the 2*p* Wyckoff site was set to 100% Y.

In Figure 2 we present the simulated diffractograms (solid lines) in the same experimental conditions used at the ESRF synchrotron source, for model Ca@Y (a) and Ca@Ba (c). In these simulations, the only significant differences between the two models are observed for small values of the scattering vector *Q*, mostly for the intensitiy of the (0 0 1) Bragg reflection, whereas for larger *Q*-values they tend to vanish. The Bragg reflections (0 1 0) and (0 0 1) show an inverse intensity relation in the two models, due to the increase of the (0 0 1) reflection by a factor of ∼3.5 when Ca sits at the Y site. Simulations of neutron diffraction patterns (not shown) with a wavelength of 1.59 Å as used in our previous work,[7] on the other hand, show no significant differences between the two models.

The experimental diffractograms collected in the ID27 beamline at the ESRF are presented in Figure 2 (b and d). Two features may be stressed from this graph. First, the intensity relation of the (0 1 0) and (0 0 1) Bragg reflections in both samples matches the model Ca@Y, that is, Ca occupying the 2*p* Wyckoff site. Second, the sample BaCa10, which was prepared assuming a nominal 10% Ca−doping at the Ba site, presents additional reflections, which do not correspond to the compound. These reflections, highlighted with arrows in Figure 2(d), correspond to segregated $YCoO_3$,[39] and were also observed in the diffractogram collected with a conventional X-ray diffractometer using Cu Kα radiation.

A full-pattern Rietveld refinement of the XRPD data was performed for samples BaCa10 (a) and YCa10 (b) and is presented in Figure 3. In both samples, the main phase is almost identical and corresponds to $(Y_{0.9}Ca_{0.1})BaCo_2O_{5.5}$ phase, that is, with Ca sharing with Y the 2*p* site. In addition, sample BaCa10 was refined adding a second phase: $YCoO_3$. The weight fraction of this phase refined to a value of 0.11,

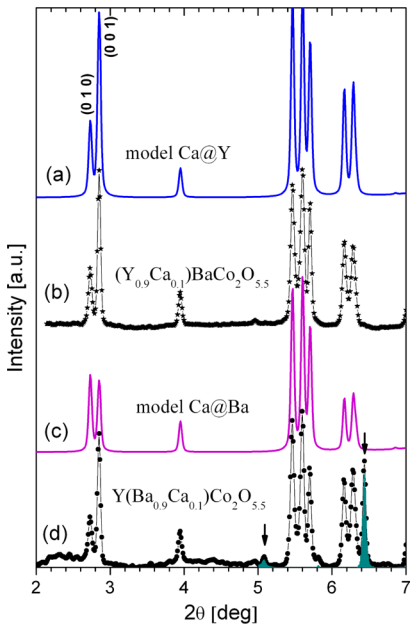

Figure 2. (a, c) Simulated X-ray powder diffractograms for model Ca@Y, corresponding to a 10 at. % Ca substitution at the crystallographic site 2*p* (a), and for model Ca@Ba with 10 at. % Ca at site 2*o* (c). (b, d) Rietveld refinement of XRPD data (λ = 0.3738 Å) with Ca occupation at sites 2*p* and 2*o* set as free parameters, corresponding to samples YCa10 (b) and BaCa10 (d). The shaded peaks in (d), marked with arrows, correspond to a second phase included in the refinement, identified as $YCoO_3$.

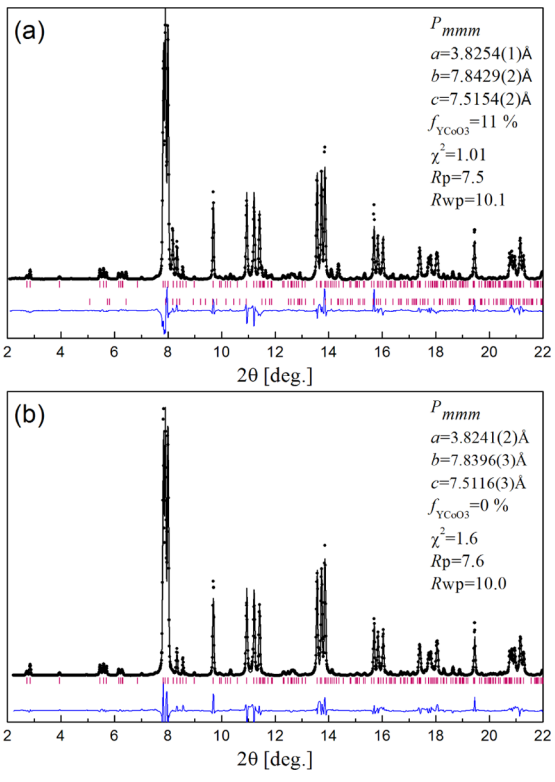

Figure 3. Rietveld refinement of samples BaCa10 (a) and YCa10 (b). Symbols correspond to experimental XRPD data and the line represents the refinement. For sample BaCa10 the best fit corresponds to a two-phase mixture of $(Y_{0.9}Ca_{0.1})BaCo_2O_{5.5}$ (first row of vertical bars at the bottom) and $YCoO_3$ (second row). The refinement of sample YCa10 was performed with a single phase $(Y_{0.9}Ca_{0.1})$-$BaCo_2O_{5.5}$. The line at the bottom of the panels correspond to the difference curve between experimental and calculated patterns.

dx.doi.org/10.1021/cm401394x | *Chem. Mater.* 2013, 25, 3307−3314

which corresponds to a mole fraction of 0.21. This value can be compared with a simple calculation based on the nominal stoichiometry

$$n(YBa_{0.9}Ca_{0.1}Co_2O_{5.5}) \rightarrow n_1(Y_{0.9}Ca_{0.1}BaCo_2O_{5.5}) + n_2(YCoO_3)$$

where n, n_1, and n_2 represent the moles of the compounds $Y(Ba_{0.9}Ca_{0.1})Co_2O_{5.5}$, $(Y_{0.9}Ca_{0.1})BaCo_2O_{5.5}$, and $YCoO_3$, respectively. Assuming that all the Ba cations go completely into $(Y_{0.9}Ca_{0.1})BaCo_2O_{5.5}$ then $n_1 = 0.9n$ and the cationic balance yields a value of $n_2 \approx 0.19 \times n$, in good agreement with the phase fraction obtained from the Rietveld refinement.

X-ray Absorption Spectroscopy. The local structure around Ca, Ba, and Co atoms was explored using XAS techniques. In Figure 4 we have sketched the room temperature

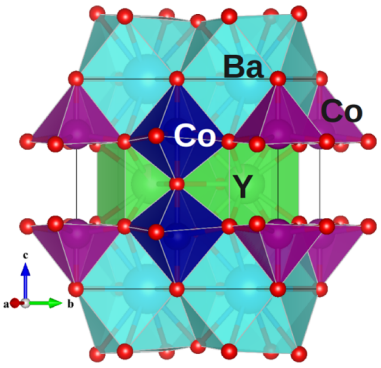

Figure 4. Crystal structure of $YBaCo_2O_{5.5}$ at room temperature as refined from our XRPD data of sample YCa10. The oxygen coordination polyhedra around the cations are represented using different colors. Co atoms are located at pyramids and octahedra in an ordered array.

crystal structure of $YBaCo_2O_{5.5}$ with emphasis on the coordination polyhedra. Due to the particular order of vacancies at $\delta = 0.5$, the Y and Ba cations have different first coordination shells: Ba atoms are coordinated with 12 oxygen neighbors at an average distance of 2.87 Å, Y atoms are coordinated with 10 oxygen atoms at an average distance of 2.51 Å, as summarized in Table 1. Therefore, the first coordination shells of the Ba and Y sites differ enough to be distinguished through X-ray absorption measurements.

Ca K-edge. The normalized XAS spectra of samples YCa10 and BaCa10 at the Ca K-edge are shown in Figure 5(a). The spectra are identical after normalization. Given that the XANES signal comes from the interaction of the photoelectron with the average atomic structure and potentials around the absorber atoms, the conclusion is that the Ca ions occupy the same crystallographic site in both samples. This is in agreement with our previous XRPD results, suggesting a unique configuration for Ca in both samples.

The two possible substitution sites ($2p$ and $2o$) were modeled using FEFF8.4 calculations to obtain the simulated XANES spectra of Ca@Y and Ca@Ba models. The experimental Ca K-edge XANES spectrum of sample BaCa10 is shown in Figure 6, together with the simulated XANES spectra. The comparison of the energy position of the absorption edges of the samples' spectra with those of the standards indicates that Ca is in the +2 oxidation state, as expected. The good match between the experimental data and

Table 1. Comparison between the Crystallographic Structure around the Ca Atom for the Ca@Ba and Ca@Y Models Calculated from the XRPD Data and the Results of the EXAFS Refinements for Samples BaCa10 and YCa10[a]

	models		EXAFS	
photoelectron path	Ca@Ba	Ca@Y	BaCa10	YCa10
	CN	CN	CN	CN
	R (Å)	R (Å)	R (Å)	R (Å)
			σ^2 (Å^2)	σ^2(Å^2)
Ca−O	12	10	10	10
	2.87	2.51	2.50(1)	2.49(2)
			0.015(5)	0.012(4)
Ca−Co	8	8	8	8
	3.33	3.30	3.30(2)	3.29(1)
			0.008(3)	0.007(2)
Ca−Ba/Y	5	5	5	5
	3.83	3.75	3.71(4)	3.70(3)
			0.013(5)	0.012(4)
Ca−O	16	16	16	16
	4.81	4.56	4.69(4)	4.67(4)
			0.006(5)	0.006(5)
			$S_0^2 = 0.8(2)$	$S_0^2 = 0.8(2)$
			$\chi_\nu^2 = 11$	$\chi_\nu^2 = 24$

[a]CN, coordination numbers; R, atomic distances; σ^2, Debye−Waller factors. The numbers between parentheses represent the error on the last digit. For Fourier filtered data the usual χ_ν^2 is multiplied by the factor $N_{ind}/(N_{ind} - N_{par})$, were N_{ind} is the number of independent points and N_{par} the number of free parameters in the fits.

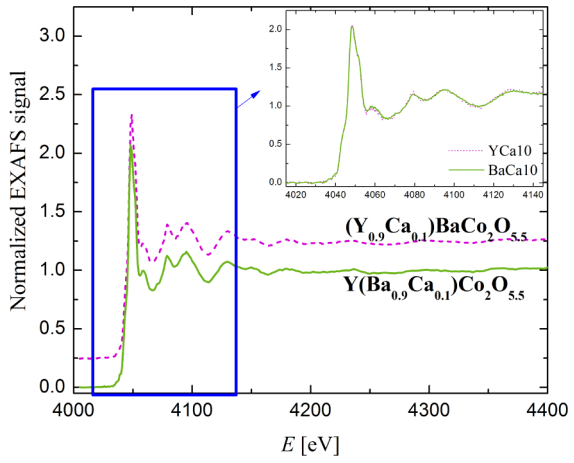

Figure 5. Normalized EXAFS spectra at Ca K-edge for samples YCa10 (nominal $(Y_{0.9}Ca_{0.1})BaCo_2O_{5.5}$) and BaCa10 (nominal $Y(Ba_{0.9}Ca_{0.1})Co_2O_{5.5}$). Spectra have been shifted vertically for easy of view. The marked area corresponds to the XANES region. Inset: XANES signal at Ca K-edge for samples YCa10 (symbols) and BaCa10 (line). No shift has been applied in this case.

the XANES signal calculated for Ca atoms located at the Y site is a strong evidence that the Ca@Y model is the most suitable to describe the system, as the Ca@Ba model is much worse. In Figure 6 we have highlighted the main features of the XANES spectrum using vertical bars, showing that they are well reproduced by simulations using the Ca@Y model.

To confirm these results, the local structure around Ca was refined fitting the extended part of the spectra (EXAFS) using our XRPD crystallographic data as starting structure. We considered up to four averaged coordination shells around Ca,

dx.doi.org/10.1021/cm401394x | *Chem. Mater.* 2013, 25, 3307−3314

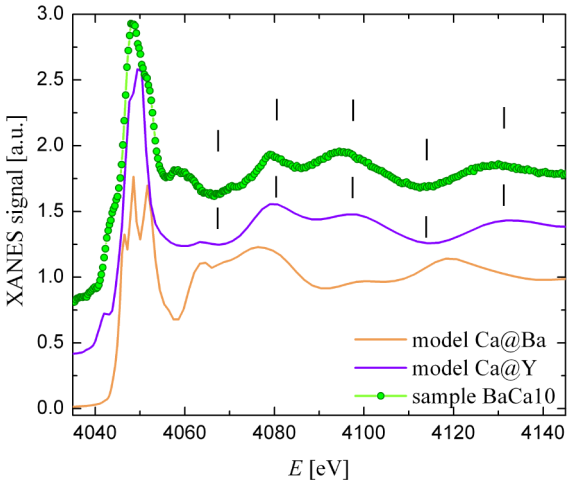

Figure 6. Simulated Ca K-edge XANES spectra the Ca@Y and Ca@Ba models. The experimental spectrum of sample BaCa10 (nominal $Y(Ba_{0.9}Ca_{0.1})Co_2O_{5.5}$) is shown for comparison using symbols. The spectra are vertically shifted for clarity. The vertical bars highlight the agreement between the main features of the sample and those of the Ca@Y model.

corresponding to Ca−O, Ca−Co, Ca−Ba(Y), and again Ca−O. The expected average distances obtained from the XRPD data refinement are shown in Table 1. The EXAFS fits were conducted in the back-Fourier transform space using four single-scattering paths for the shells above-mentioned. The extracted EXAFS signal for sample YCa10 and the best fit curve are shown in Figure 7(a). The signal from each shell is also shown, vertically shifted for clarity. The representation of the experimental data and fit curve in the Fourier transform space R is shown in Figure 7(b), where each shell can be identified.

The structural parameters extracted from the EXAFS fits at the Ca K-edge are summarized in Table 1, together with the structure calculated from the Ca@Y and Ca@Ba models. The comparison shows that the experimental data clearly match the model where Ca is located at the Y site.

Ba L-edges. To check the consistency of the results, the same analysis was applied to data collected at the Ba L_{III} and Ba L_I edges. The comparison of the XANES spectra of the YCa10 and BaCa10 samples at the Ba L_{III}-edge again reveals that the local structure around Ba is identical for the two samples, as illustrated in Figure 8.

For the EXAFS analysis, we switched to the L_I edge to reduce absorption and obtain better spectra. The analysis was only performed on the BaCa10 sample, as we had already verified that both samples had identical absorption spectra at the L_{III} edge.

The EXAFS signal for sample BaCa10 and the best fit curve are shown in Figure 9(a), together with the signals from each coordination shell. The Fourier transformed EXAFS data and the corresponding fit curve are shown in Figure 9(b). The extracted structural parameters, which are summarized in Table 2, are in good agreement with the long-range structure coming from XRPD measurements. The observed mismatches in the structural parameters are normal when comparing crystallographic and local structure data and can arise from a different arrangement of the atoms within the unit cell. The results indicate that the local structure observed around the Ba atom is definitively different from the one observed around host Ca

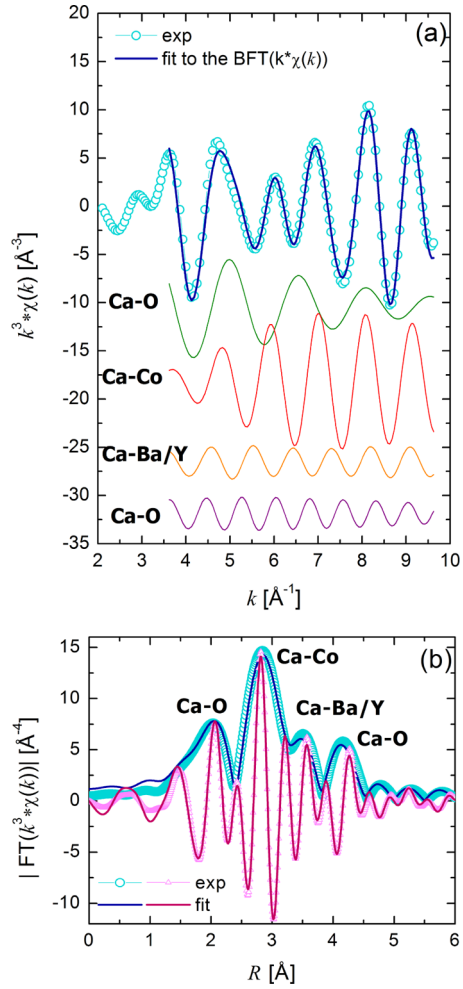

Figure 7. (a) Back Fourier transformed (1.4−4.8 Å) Ca K-edge EXAFS signal of sample YCa10 ($(Y_{0.9}Ca_{0.1})BaCo_2O_{5.5}$). Symbols correspond to the experimental data and solid lines represent the fit curves. The contributions of each scattering path are also shown (vertically shifted). (b) Fourier transform (4−10 $Å^{-1}$, Gaussian window) of the Ca K-edge EXAFS signal (symbols) of sample YCa10 and of the corresponding fit curve (solid lines). The four coordination shells considered in the fit are indicated in the graph. Triangles represent the imaginary part of the Fourier transform. The Fourier transform is k^3-weighted and is shown not corrected for the phase shift.

atoms, confirming that Ba and Ca do not share the same crystallographic sites.

Co K-edge. Since all evidence leads to the conclusion that Ca substitutes at the Y site, we must consider the charge balance issue. In our previous work, we had assumed that Ca, located at the Ba site, has no influence on the electronic doping being both cations in a +2 oxidation state. However, the present work proves that Ca^{2+} replaces Y^{3+}; therefore, a higher Co valency is needed to preserve charge balance. Special care must be taken regarding the oxygen stoichiometry in the following discussion. We have shown in previous works[6,7] that Ca addition does not modify the oxygen stoichiometry of our samples when prepared in the same batch. This was precisely determined from the refinement of oxygen occupation from high−resolution neutron diffraction data.[7] The present samples were prepared under identical conditions of temperature, time, and oxygen flow; and therefore, we expect the same oxygen stoichiometry ($\delta \simeq 0.47 - 0.5$). This was confirmed by the magnetic and

dx.doi.org/10.1021/cm401394x | *Chem. Mater.* 2013, 25, 3307−3314

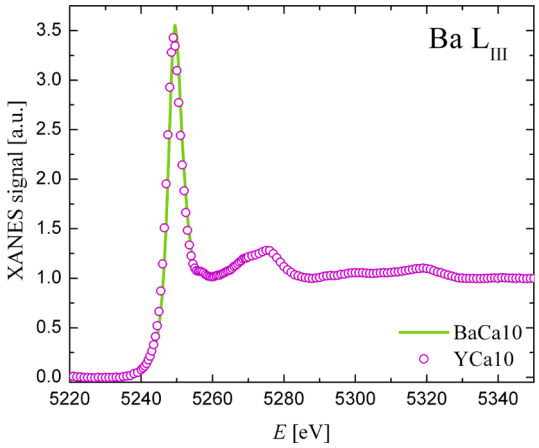

Figure 8. Normalized XANES spectra at Ba L_{III}-edge for samples YCa10 (nominal $(Y_{0.9}Ca_{0.1})BaCo_2O_{5.5}$) and BaCa10 (nominal $Y(Ba_{0.9}Ca_{0.1})Co_2O_{5.5}$).

electrical characterization (not shown) in excellent agreement with our previously published results,[6,7] as well as those from M. Seikh et al.[23] and Sarkar et al.[11] Having said this, let us now examine the valence state of cobalt. It has been proposed that, even when the nominal valence of Co is 3+, there must exist a disproportionation into Co^{2+} and Co^{4+}, possibly located near the Ca atoms, for the Co^{3+}−O−Co^{4+} FM superexchange interactions to account for the ferrimagnetic/AFM competition observed.[19] In the present samples, in which Y^{3+} is replaced by Ca^{2+}, the nominal Co valence is in fact higher than 3+ and so the ferrimagnetic behavior can be naturally explained by the formation of Co^{4+} induced by Ca. A similar effect is observed in Sr-doped $La_{1-x}Sr_xCoO_3$, in which the substitution of Sr^{2+} for La^{3+} induces the formation of Co^{4+} that is claimed to be responsible for the enhancement of ferromagnetic interactions.

To check the presence of Co^{4+} in our samples, we analyzed the Co K-edge XANES data collected at the ESRF. Following previous works on similar Co-based perovskites,[40,41] we focused on the pre-edge peak situated around 7711 eV, which is attributed to $1s \rightarrow 3d$ transitions and carries information on the occupation of t_{2g} and e_g orbitals. This electronic transition, usually forbidden, can be experimentally observed due to the heavy admixture of cobalt's 3*d* orbitals with oxygens' 2*p* ones. The second derivative of the pre-edge peak has been shown to reveal two features, separated by ∼2.3 eV, which are related to the crystal field splitting of the t_{2g} and e_g orbitals.[40,41]

In Figure 10(a), we show the normalized Co K-edge XANES spectra of samples YCa10, BaCa10, and of two references samples, $LaCoO_3$ (Co^{3+}) and $BaCoO_3$ (Co^{4+}) (the latter after ref 42). The pre-edge region of interest is enlarged and shifted for clarity in panel (b). The baseline subtracted pre-edge peaks for the two reference compounds and our two samples are plotted using symbols in Figure 11. For the $LaCoO_3$ reference (a), the pre-edge peak was fitted using two Gaussian functions, separated by ∼2 eV and centered at 7710 and 7712 eV. The second derivative of the fit is shown using dashed lines. It can be seen that the two features usually associated to the t_{2g} and e_g orbitals are well resolved, and their shape and location agree with previous reports.[41] On the other hand, only one Gaussian function was enough to fit the pre-edge peaks of the YCa10, BaCa10, and $BaCoO_3$ pre-edge peaks. In these, the peak is broader and centered at 7710.0 eV; that is, there is a shift

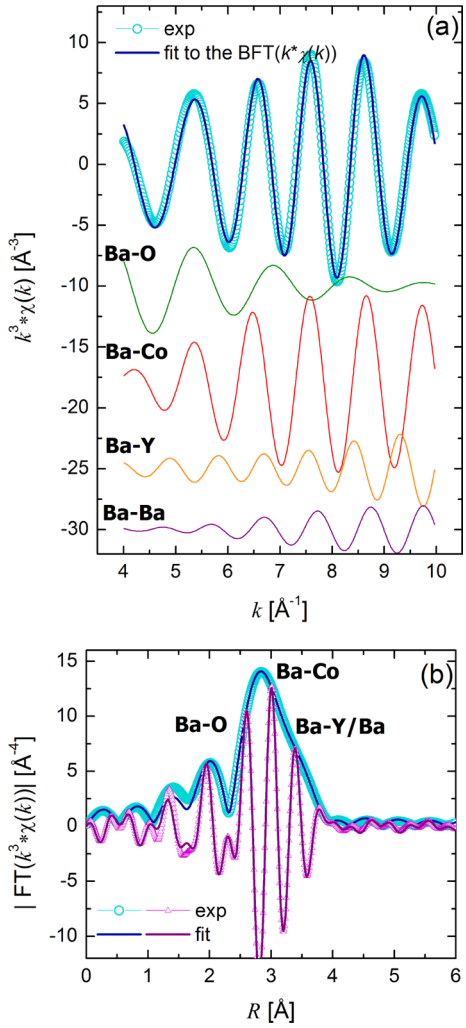

Figure 9. (a) Back Fourier transformed (1.6−3.8 Å) L_I Ba-edge EXAFS signal of sample BaCa10 ($Y(Ba_{0.9}\ Ca_{0.1})Co_2O_{5.5}$). The symbols correspond to the data and the line to the fit. The contributions of each scattering path are shown vertically shifted. (b) Fourier transform (3.6−10 $Å^{-1}$, Gaussian window) of the Ba L_I-edge EXAFS signal (symbols) of sample BaCa10 and of the corresponding fit curve (solid lines). The four coordination shells considered in the fit are indicated in the graph. Triangles represent the imaginary part of the Fourier transform. The Fourier transform is k^3-weighted and is not corrected for the phase shift.

toward the lower energy (t_{2g}) feature. The same tendency is actually observed when doping $LaCoO_3$ with Sr^{2+}, as a result of the high-spin Co^{3+} substitution with low-spin Co^{4+}.[40] Therefore, this analysis gives further support to the Co^{4+} substitution for Co^{3+}.

■ CONCLUSIONS AND FINAL REMARKS

The layered cobaltites $RBaCo_2O_{5.5}$ continue to be a matter of numerous investigations. Cation substitution has proven to trigger even more interesting questions regarding the phase competition in the system, as it deeply affects their magnetism. It has been recently proposed that the Ca-doped compound exhibits features of magnetic glassiness,[11] regardless of the substitution site. This possibility deserves further magnetic characterizations using controlled protocols, which are under progress. It is possible that the history-dependent magnetic state of the system can account for a number of confuse reports

dx.doi.org/10.1021/cm401394x | Chem. Mater. 2013, 25, 3307−3314

Table 2. Comparison between the Crystallographic Long-Range Structure around a Ba Atom Obtained from XRPD and the Local Structure Obtained from the EXAFS Refinement of the Ba L_I-edge for Sample BaCa10[a]

photoelectron path	XRPD model	EXAFS fit
	CN	CN
	R (Å)	R (Å)
		σ^2 (Å^2)
Ba−O	12	12
	2.92	2.65(1)
		0.012(5)
Ba−Co	8	8
	3.33	3.30(1)
		0.003
Ba−Y	2	2
	3.75	3.66(1)
		0.005
Ba−Ba	4	4
	3.87	3.84(1)
		0.005
		S_0^2 = 1.6(3)
		χ_ν^2 = 57

[a]CN, coordination numbers; R, atomic distances; σ^2, Debye−Waller factors). The numbers between parentheses represent the error on the last digit. For Fourier filtered data the usual χ_ν^2 is multiplied by the factor $N_{ind}/(N_{ind} - N_{par})$, were N_{ind} is the number of independent points and N_{par} the number of free parameters in the fits.

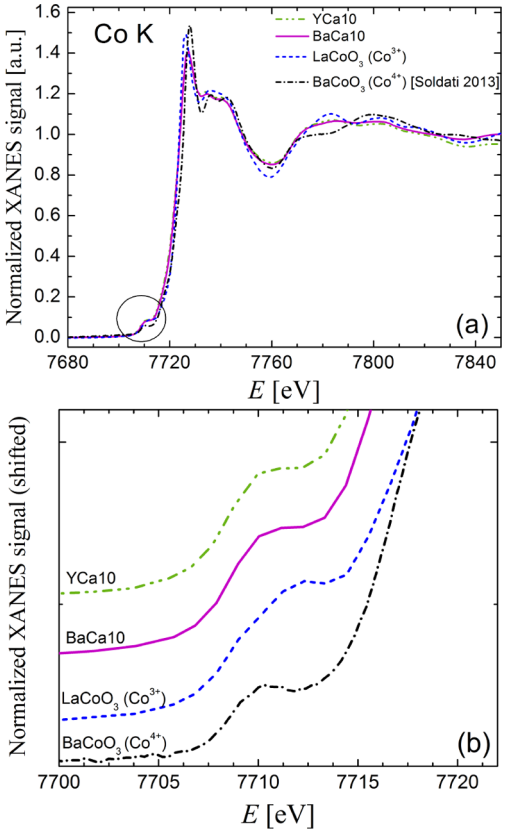

Figure 10. Normalized Co K-edge XANES signal for samples BaCa10 ($Y(Ba_{0.9}Ca_{0.1})Co_2O_{5.5}$), YCa10 ($(Y_{0.9}Ca_{0.1})BaCo_2O_{5.5}$), as well as two reference samples: $LaCoO_3$ (Co^{3+}) and $BaCoO_3$ (Co^{4+}) after Soldati et al.[42] The inset shows a magnified region of the pre-edge peak.

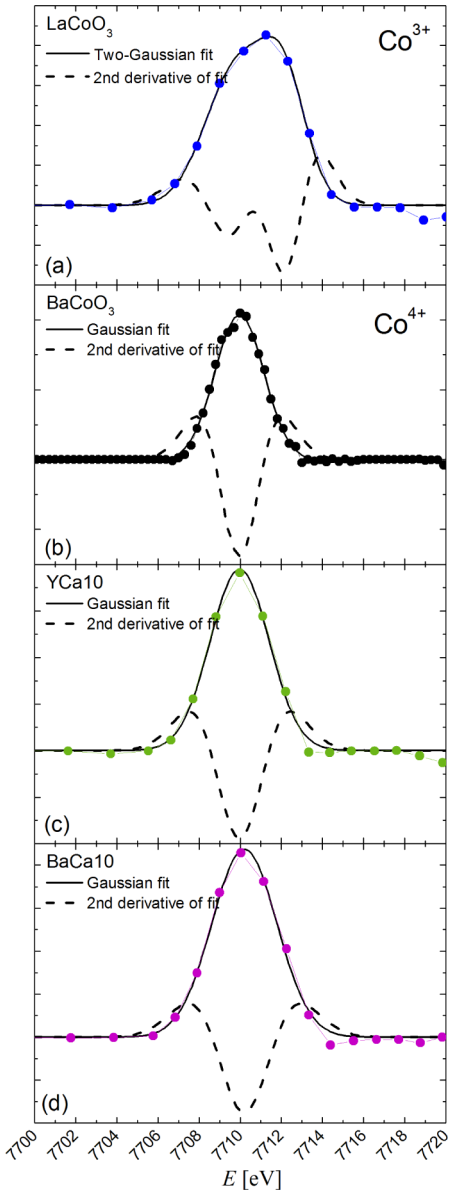

Figure 11. Baseline subtracted pre-edge peak (symbols), peak fit using Gaussian functions (solid lines), and second derivative of fit (dashed lines) for the reference compounds $LaCoO_3$ and $BaCoO_3$[42] (a, b), as well as samples YCa10 and BaCa10 (c, d).

in the literature. Anyway, the accurate knowledge of the substitution site remained a standing issue, and is of crucial importance to understand the magnetic phenomena.

In this work, we have thoroughly revised the cationic arrangements in Ca-doped layered cobaltites, making use of a local and chemically selective probe as XAS, combined with synchrotron radiation XRPD and simulations. By applying a multitechnique approach, we have ruled out the possibility that Ca substitutes at the Ba site, and confirmed that the substitutional site is the Y one. In addition, we also reported experimental evidence supporting the presence of Co^{4+} in the Ca-doped samples. Thanks to these results, the scenario in which the ferromagnetic arrangement is due to the occurrence of Co^{4+} ions, gains support. The present study represents a major contribution toward clarifying the underlying mechanisms for the ferrimagnetic enhancement in Ca-doped $YBaCo_2O_{5.5}$.

dx.doi.org/10.1021/cm401394x | Chem. Mater. 2013, 25, 3307−3314

AUTHOR INFORMATION

Corresponding Author

*E-mail: gaurelio@cab.cnea.gov.ar.

Notes

The authors declare no competing financial interest.

ACKNOWLEDGMENTS

This work has been partially supported by the Argentina−Italy collaboration program MAE-MinCyT. Financial support was also received from LNLS to carry the XAS experiments. We thank the responsible of the GILDA beamline at the ESRF, Francesco D'Acapito, and the Italian responsible for the Argentina−Italy collaboration program, Settimio Mobilio. Virginia Tognoli and Ruben Benavides from CAB are gratefully acknowledged for technical support. We also thank Leandro Acuña and Analía Soldati for making their $BaCoO_3$ XANES data available to us.

REFERENCES

(1) Vogt, T.; Woodward, P.; Karen, P.; Hunter, B.; Henning, P.; Moodenbaugh, A. *Phys. Rev. Lett.* **2000**, *84*, 2969.

(2) Suard, E.; Fauth, F.; Caignaert, V.; Mirebeau, I.; Baldinozzi, G. *Phys. Rev. B* **2000**, *61*, R11871−R11874.

(3) Akahoshi, D.; Ueda, Y. *J. Phys. Soc. Jpn.* **1999**, *68*, 736−739.

(4) Moritomo, Y.; Akimoto, T.; Takeo, M.; Machida, A.; Nishibori, E.; Takata, M.; Sakata, M.; Ohoyama, K.; Nakamura, A. *Phys. Rev. B* **2000**, *61*, R13325−R13328.

(5) Frontera, C.; García-Muñoz, J.; Llobet, A.; Aranda, M. *Phys. Rev. B* **2002**, *65*, 180405.

(6) Aurelio, G.; Curiale, J.; Sánchez, R. D.; Cuello, G. J. *Phys. B: Condens. Matter* **2007**, *398*, 223−228.

(7) Aurelio, G.; Curiale, J.; Sánchez, R. D.; Cuello, G. J. *Phys. Rev. B* **2007**, *76*, 214417.

(8) Khalyavin, D.; Argyriou, D.; Amann, U.; Yaremchenko, A.; Kharton, V. *Phys. Rev. B* **2008**, *77*, 064419.

(9) Luetkens, H.; Stingaciu, M.; Pashkevich, Y.; Conder, K.; Pomjakushina, E.; Gusev, A.; Lamonova, K.; Lemmens, P.; Klauss, H.-H. *Phys. Rev. Lett.* **2008**, *101*, 017601.

(10) Aurelio, G.; Curiale, J.; Sánchez, R. D.; Cuello, G. J. *J. Phys.: Condens. Matter* **2009**, *21*, 326002.

(11) Sarkar, T.; Pralong, V.; Raveau, B. *Phys. Rev. B* **2011**, *83*, 214428.

(12) Kolesnik, S.; Dabrowski, B.; Chmaissem, O.; Avci, S.; Hodges, J.; Avdeev, M.; Świerczek, K. *Phys. Rev. B* **2012**, *86*, 064434.

(13) Zhang, X.; Hao, H.; Hu, X. *Phys. B: Condens. Matter* **2008**, *403*, 3406−3409.

(14) Tarancón, A.; Burriel, M.; Santiso, J.; Skinner, S. J.; Kilner, J. A. *J. Mater. Chem.* **2010**, *20*, 3799.

(15) Motohashi, T.; Ueda, T.; Masubuchi, Y.; Takiguchi, M.; Setoyama, T.; Oshima, K.; Kikkawa, S. *Chem. Mater.* **2010**, *22*, 3192−3196.

(16) Song, H.; Qin, Z.; Gao, F.; Jia, J.; Yang, D.; Hu, X. *Sens. Actuators, B* **2013**, *177*, 50−54.

(17) Thirumurugan, N.; Bharathi, A.; Arulraj, A.; Sundar, C. *Mater. Res. Bull.* **2012**, *47*, 941−946.

(18) Thirumurugan, N.; Amaladass, E.; Sundar, C.; Bharathi, A. Magnetic glass-like arrest in Ca-doped $GdBaCo_2O_{5.53}$. *AIP Conference Proceedings*, 2012; p 1203

(19) Motin Seikh, M.; Kundu, A. K.; Caignaert, V.; Pralong, V.; Raveau, B. *J. Appl. Phys.* **2011**, *109*, 093916−093916.

(20) Zhang, X.; Jin, M. *J. Power Sources* **2010**, *195*, 1076−1078.

(21) Motin Seikh, M.; Caignaert, V.; Pralong, V.; Raveau, B. *Solid State Commun.* **2009**, *149*, 697−702.

(22) Kim, J. H.; Cassidy, M.; Irvine, J. T. S.; Bae, J. *J. Electrochem. Soc.* **2009**, *156*, B682.

(23) Motin Seikh, M.; Raveau, B.; Caignaert, V.; Pralong, V. *J. Magn. Magn. Mater.* **2008**, *320*, 2676−2681.

(24) Motin Seikh, M.; Caignaert, V.; Pralong, V.; Simon, C.; Raveau, B. *J. Phys.: Condens. Matter* **2008**, *20*, 015212.

(25) Pechini, M. U.S. Patent No. 3.330.697, 1967.

(26) Hammersley, A. P.; Svensson, S. O.; Hanfland, M.; Fitch, A. N.; Hausermann, D. *High Pressure Res.* **1996**, *14*, 235−248.

(27) Rodríguez-Carvajal, J. FULLPROF: A program for Rietveld Refinement and Pattern Matching Analysis. *Abstracts of the Satellite Meeting on Powder Diffraction of the XV Congress of the IUCr*, Toulouse, France, 1990; p 127.

(28) Cazorla-Amoros, D.; Linares-Solano, A.; Salinas-Martinez de Lecea, C.; Nomura, M.; Yamashita, H.; Tomita, A. *Energy Fuels* **1993**, *7*, 625−631.

(29) Pascarelli, S.; Boscherini, F.; d'Acapito, F.; Hrdy, J.; Meneghini, C.; Mobilio, S. *J. Synchrotron Radiation* **1996**, *3*, 147−155.

(30) Rehr, J.; Albers, R. *Rev. Mod. Phys.* **2000**, *72*, 621.

(31) Monesi, C.; Meneghini, C.; Bardelli, F.; Benfatto, M.; Mobilio, S.; Manju, U.; Sarma, D. *Phys. Rev. B* **2005**, *72*, 174104.

(32) Meneghini, C.; Bardelli, F.; Mobilio, S. *Nucl. Instrum. Methods Phys. Res., Sect. B* **2012**, *285*, 153−157.

(33) Bardelli, F.; Meneghini, C.; Mobilio, S.; Ray, S.; Sarma, D. *J. Phys.: Condens. Matter* **2009**, *21*, 195502.

(34) James, F.; Roos, M. *Comput. Phys. Commun.* **1975**, *10*, 343−367.

(35) Ankudinov, A.; Ravel, B.; Rehr, J.; Conradson, S. *Phys. Rev. B* **1998**, *58*, 7565.

(36) Ankudinov, A.; Bouldin, C.; Rehr, J.; Sims, J.; Hung, H. *Phys. Rev. B* **2002**, *65*, 104107.

(37) Newville, M.; Ravel, B.; Haskel, D.; Rehr, J.; Stern, E.; Yacoby, Y. *Phys. B: Condens. Matter* **1995**, *208*, 154−156.

(38) Stern, E. *Theory of EXAFS, X-Ray Absorption Principles, Applications Techniques of EXAFS, SEXAFS, and XANES*; Königsberger and Prins: New York, 1988.

(39) Knížek, K.; Jirák, Z.; Hejtmánek, J.; Veverka, M.; Maryško, M.; Hauback, B. C.; Fjellvåg, H. *Phys. Rev. B* **2006**, *73*, 214443.

(40) Efimov, V.; Efimova, E.; Karpinsky, D.; Kochubey, D. I.; Kriventsov, V.; Kuzmin, A.; Molodtsov, S.; Sikolenko, V.; Tiutiunnikov, S.; Troyanchuk, I. O.; Shmakov, A. N.; Vyalikh, D. *Phys. Status Solidi (C)* **2007**, *4*, 805−808.

(41) Haas, O.; Struis, R.; McBreen, J. *J. Solid State Chem.* **2004**, *177*, 1000−1010.

(42) Soldati, A. L.; Baqué, L.; Napolitano, F.; Serquis, A. *J. Solid State Chem.* **2013**, *198*, 253−261.